A Study on Truncated Cone-beam Sampling Strategies for 3D Mammography

Junhai Wen, Hongbing Lu, Wei Zhao, Zigang Wang, and Zhengrong Liang, *Member, IEEE*

***Abstract* -- In USA, breast cancer is a most frequent cause of deaths for women. It is important to detect the cancer in its early stage. X-ray three-dimensional (3D) mammography can provide a good image resolution and contrast. However, the associated radiation is relative high. Reduction of the soft X-ray radiation for 3D mammography has been a research focus in the past years. In a typical 3D mammography system, the X-ray source and detector rotate around the object (breast) beneath the table, on which the patient lies in a prone position. In order to sample the data as close as possible to the chest base, a circular orbit with half cone-beam geometry has been investigated. It can provide very good reconstruction if the X-ray source is far away from the object. For a relative short distance between the source and the object for an improved spatial resolution, the circular orbit may not be an optimal choice. In this case, the portion far away from the circular orbit wouldn't be well reconstructed because of the missing of projection data in that region. In this work, we investigated five possible orbits, attempting to find an optimal orbit that can reconstruct satisfactorily the whole object with least projections (less radiation). The results showed that two near half-circular orbits may be a choice, one near the chest base and the other near the breast tip. The redundant samplings beyond 180o were eliminated by our algorithm, rendering very good reconstructions.**

I. INTRODUCTION

Breast cancer is the most frequent cause of deaths for women in USA. Women have a much better chance of surviving breast cancer if the disease can be detected early. Mammography has been playing a major role in the early detection. However, it is far from perfect [1, 2]. Although advanced digital mammography with excellent spatial resolution and tissue contrast is currently available as a screening modality with very sophisticated computer-aided detection (CAD) means to help radiologists to identify any malignant abnormality, the accuracy and/or specificity is still relatively low. One major problem with mammography is that in the projected two-dimensional (2D) image from 3D compressed object, anatomical structures can overlap and possibly impede visualization of diagnostic information. In addition, the morphologic characteristics of micro-calcifications clusters -- an important diagnostic indicator in mammography -- can be distorted by compressing the breast and projecting the 3D calcification pattern onto a 2D plane. Removal of the tissue-overlap limitation of the conventional 2D digital mammography for a fully 3D mammography has been attempted by many researchers in the past years across the world. 3D mammography can provide both a fully 3D image of the breast and any 2D projection image of the 3D object. It is hoped that the 3D information will improve the diagnosis and surgical intervention [1-3].

With recent advancement in digital detector technologies, reconstruction of a 3D high resolution, high contrast image of the breast from 2D projections, which are adequately sampled around the object, could be achieved by currently available computer tomography (CT) technologies. But the increased radiation dosage by multiple projections limits its clinical applications as a screening modality. Reduction of the soft X-ray radiation for 3D mammography has been a research focus in the recent years. We have been interested in software approaches to achieve the same goal of minimizing the radiation. In our preliminary studies on low-dose CT technologies [4-6], we have shown that our algorithm can achieve at least three times reduction of the X-ray exposure, as compared to currently available CT technologies. In this work, we investigated five possible orbits, attempting to find an optimal orbit that can reconstruct satisfactorily the whole object with least projections (less radiation). The results showed that two near half-circular orbits might be a choice, one near the chest base and the other near the breast tip. In our modified cone-beam reconstruction algorithm, the redundant samplings beyond 180^{o} were eliminated, rendering very good reconstructions.

Manuscript submitted on October 20, 2003. This work was supported in part by NIH National Heart, Lung and Blood Institute under Grant No. HL54166 and the NIH National Cancer Institute under Grant No. CA82402.

J. Wen is with the Department of Radiology, State University of New York, Stony Brook, NY 11794, USA (telephone: 631-444-7999, e-mail: wenjh@mil.sunysb.edu).

H. Lu is with the Department of Radiology, State University of New York, Stony Brook, NY 11794, USA, and with the Department of Biomedical Engineering, The Fourth General Medical College, Xi'An, China.

W. Zhao and Z. Wang are with the Department of Radiology, State University of New York, Stony Brook, NY 11794, USA.

Z. Liang is with the Departments of Radiology and Computer Science, State University of New York, Stony Brook, NY 11794, USA.

II. 3D MAMMOGRAPHY SYSTEM

A. A typical X-ray 3D mammography system

A typical X-ray 3D mammography system is showed in Figure 1, which has been accepted in the research field [2]. The patient lies prone on a table, and the unimpressed breast hangs through a hole in the table. The detector and X-ray source are set under the patient table and rotate around the vertical axis of the object (breast) to acquire 2D projection data. The X-ray source and detector are restricted by the table, so the breast is exposed to the X-rays in a half cone-beam geometry if the X-ray source rotates closest to the table, or in a truncated cone-beam geometry if the source moves away from the table.

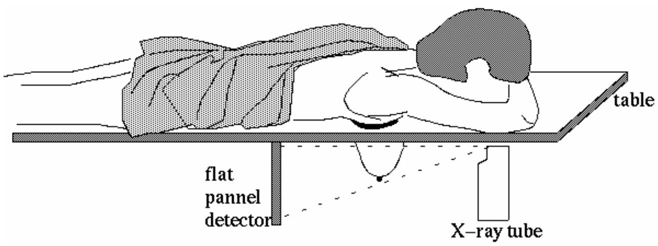

Figure 1: A prototype of 3D mammography system with a collimated X-ray source and high spatial resolution, high detection efficiency flat-panel detector [2], where the source-detector distance is 72 cm and the source is 48 cm from the center of the object. For improved spatial resolution detection efficiency, a shorter distance between source and object may be used.

B. Mathematical breast phantom

A 3D mathematical breast phantom is showed in Figure 2. The phantom is a half-ellipsoid (see Figure 2(d)), just like the breast hanging through the hole in the table. The phantom has an array size of 512x512x512 voxels. Within the phantom, there are three groups of objects that locate in three transverse planes, whose distances to the table (the top of phantom) are 52, 176, 296 voxels, respectively (see Figures 2(a), 2(b), 2(c)).

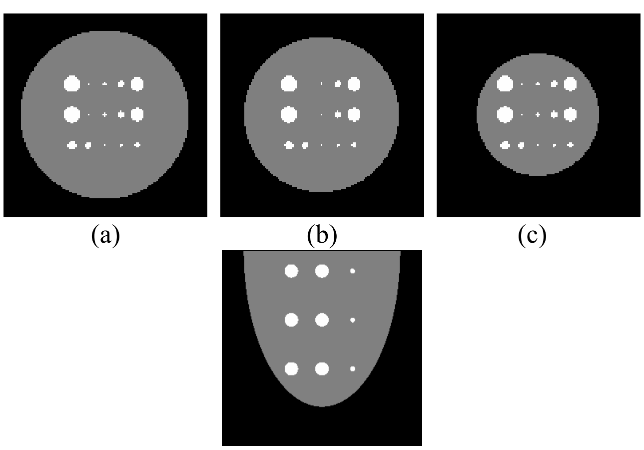

Figure 2: A 3D mathematical breast phantom, where the hot spots simulating the calcification are embedded in the background of "fat" tissue.

C. Image reconstruction algorithm

In this work, we will adapt and modify the generalized Feldkamp cone-beam reconstruction algorithm as developed by Ge Wang, *et al.* [7, 8] to fit into our scanning orbit and data acquisition geometry.

$$i(x,y,z)=\frac{1}{2}\int_0^{2\pi}\frac{\rho^2(\beta)}{(\rho(\beta)-s)^2}\int_{-\infty}^{\infty}\frac{\rho(\beta)}{\sqrt{\rho^2(\beta)+p^2+\zeta^2}}d_c(\beta,p,\zeta)\, f\left(\frac{\rho(\beta)t}{\rho(\beta)-s}-p\right)dp\,d\beta \quad (1)$$

where $i(x,y,z)$ is a 3D image, $d_c(\beta,p,\zeta)$ is the cone-beam projection data, $f(\cdot)$ is a reconstruction filter, $\rho(\beta)$ is the distance between the x-ray source and the z-axis of the reconstruction coordinate system, and β is the rotation angle of the x-ray source. The coordinates are: $t=x\cos\beta+y\sin\beta$, $s=-x\sin\beta+y\cos\beta$.

III. FIVE POSSIBLE SAMPLING ORBITS AND CHOICE OF SCANNING METHODS

In order to sample the data as close as possible to the chest base, a circular orbit with half cone-beam geometry has been investigated. It can provide very good reconstruction if the X-ray source is far away from the object. For a relative short distance between the source and the object for an improved spatial resolution and detection efficiency, the circular orbit may not be an optimal choice. In this case, the portion far away from the circular orbit wouldn't be well reconstructed because of the missing or insufficient sampling of projection data in that region. In this work, we tested five possible sampling orbits for the prototype system of Figure 1:

1) *Circular orbit*: The source rotates on a circle orbit close to the table or the cheat base. The detector remains on the circular orbit near the table for all possible sampling strategies.
2) *Spiral orbit*: The initial source location is close to the table, when scan finishes (over 360^o), it is near the breast tip or nipple.
3) *Two near half-circular orbits*: In this sampling, one near half-circular (180^o plus a fan-angle) orbit is at the chest base (close to the table) and the other near half-circular (180^o plus fan-angle) orbit is near the breast tip.
4) *Two half-spiral orbits*: One half-spiral orbit of 180^o plus a fan-angle is applied starting from the chest base. The other half-spiral orbit of 180^o plus fan-angle starts at the breast tip back to the chest base.
5) *A half circular plus a half spiral orbits*: In this sampling, one near half-circular (180^o plus a fan-angle) orbit at the chest base is applied and then a half-spiral orbit is applied from the chest base to the breast tip.

Because the detector and source are set under the patient table and rotate around the object (breast) to acquire projection data, the detector and source are limited by the patient table.

The portion of the object that is near the table will obtain less projection rays than the portion far away from the table when X-ray source moves away from the table. If we don't normalize the sampled rays, the reconstructed image will be very dark in the portion of the object that is near the table. The following formula shows our normalization technique.

$$\text{reconstructed point (nomalized)} = \frac{\text{reconstructed point}}{\text{the number of the projections that through this point}} \quad (2)$$

The reconstruction results of the five orbits are showed in Figure 3, where the distance between the source and the object is 1600 voxels and the size of phantom is 512x512x512 voxels. From these reconstructed images, we observed that the dual near half-circular orbits might be the best choice for the 3D mammography system.

IV. MODIFIED RECONSTRUCTION ALGORITHM FOR THE DUAL NEAR HALF-CIRCULAR ORBITS

Why do we choice two "near" half-circular orbits, rather than two half-circular orbits? (Near half-circular orbit means 180^o plus a fan-angle scanning). To answer this question, we introduce a sampling map, which describes the sampling (projection) status in the mid-plane of cone-beam geometry. In the mid-plane of cone-beam configuration, the geometry is a fan-beam type. The relation between fan-beam and parallel-beam geometries is showed in Figure 4.

$$\phi = \beta + \gamma = \beta + \arctan\frac{p}{D}$$

$$x_r = p\cos\gamma = \frac{pD}{\sqrt{D^2 + p^2}}. \quad (3)$$

It means that each ray (p,β) in the fan-beam geometry can be seen as a ray in the parallel-bean geometry. So in the sampling map, each ray (p,β) is one point, whose location is (ϕ, x_r). For parallel-beam geometry, after 180^o scan, the sampling map is filled by the sampling points (projection), which means that we can reconstruct image by using only the 180^o parallel-beam scans. But for fan-beam geometry, after 180^o scan (See Figure 5(a)), sampling map is not filled by the 180^o fan-beam scan (See Figure 5(c)). Some projections are missed.

To fill in these missing projection-data region, the rotating angle should be more than 180^o. The angle of added extra scans should be 2θ, where θ is the maximum open angle in fan-beam scan (See Figure 5(a) and 5(b)). But the added projections beyond 180^o will cause the redundancy of sampling (see Figure 5(d)), which could result in artifacts in the reconstructed images.

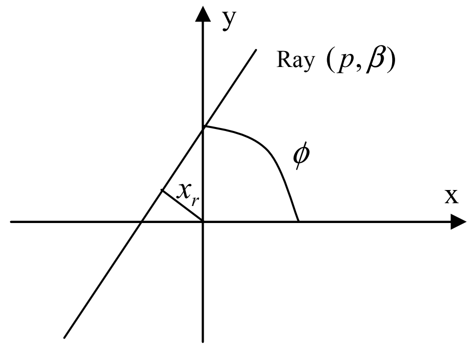

Figure 4: Relation between fan-beam and parallel-beam geometries.

In our modified image reconstruction algorithm, these redundant samplings in the added projections were eliminated. From Figure 5(d), we can see that the number of redundant samplings is different in different views. We will use the following formula to eliminate the redundant samplings.

$$L = [(D_{size}/2)(\beta - \pi)]/(2\theta) \quad (4)$$

$$\begin{cases} projection[i] = projection[i], if\,(i - D_{size}/2) > L \\ projection[i] * \exp[-0.001*(\beta-\pi)*(i - D_{size}/2 - L)^2], else \end{cases}$$

where D_{size} is the size of detector, L is the cut point which separates the useful added samplings and redundant samplings in different view β. The redundant samplings could not be eliminated directly, which would cause some artifacts. We will use Gaussian function to smooth the eliminating processing.

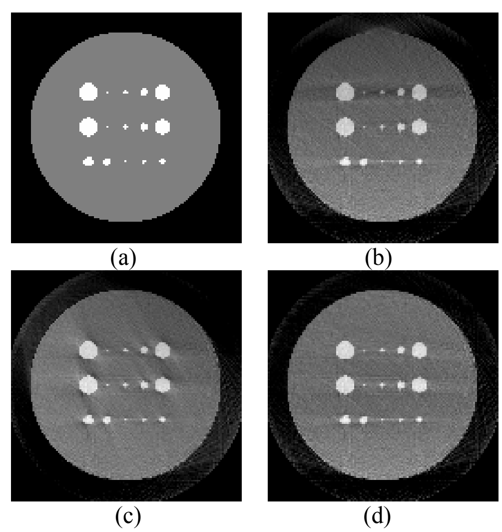

Figure 6: Reconstruction results of different compensation methods in the dual half-circular orbits. (a) phantom, (b) dual half-circular orbits without added projections, (c) dual near half-circular orbits with added projections, and (d) dual near half-circular orbits with added projections, where the redundant part was eliminated.

When the distance between the source and the object is relative short, e.g., 200 pixels, we observed that there is a missing area on the top of the reconstructed image of the dual half-circular orbits (see Figure 6(b)). This is caused by the missing projections when the 180^o cone-beam scan is applied. When these missing projection data were filled in by added extra scans, the added projections beyond 180^o would cause the redundancy of sampling, which could result in artifacts in the reconstructed image (see Figure 6(c)). Our modified image reconstruction algorithm considers this problem. After these redundant samplings in the added projections were eliminated, good reconstruction results were obtained (see Figure 6(d) and Figure 5(e)).

V. CONCLUSIONS

In this work, we investigated five possible scan orbits for 3D mammography application, and found that the dual near half-circular orbits might be the best choice, where one orbit is close to the chest base and the other is near the breast tip. A near half-circular orbit means an 180^o plus a fan-angle scan. The added projections beyond 180^o scan cause the redundancy of data sampling, which could result in artifacts in the reconstructed images. We investigated and modified the generalized Feldkamp cone-beam reconstruction algorithm to accommodate the variable scan orbits. Our modified algorithm eliminated the redundant samplings in the added projections and produced good reconstruction results.

VI. REFERENCES

[1] X. Gong, A.A. Vedula, and S.J. Glick, "An investigation of microcalcification detection using cone beam CT mammography with a flat panel imager", Proceedings of the VIIth International Conference on Fully 3D Reconstruction In Radiology and Nuclear Medicine, 2003.

[2] J. Boone, T. Nelson, K. Lindfors, and J. Seibert, "Dedicated breast CT: Radiation dose and image quality evaluation", Radiology, vol. 221, pp. 657-667, 2001.

[3] H. Barrett and W. Swindell, Radiological Imaging, Academic Press, New York, 1969.

[4] H. Lu, I-T. Hsiao, X. Li, and Z. Liang, "Noise properties of low-dose CT projections and noise treatment by scale transformations", Conference Record of IEEE NSS and MIC, in CD-ROM, 2001.

[5] H. Lu, X. Li, I-T. Hsiao, and Z. Liang, "Analytical treatment of noise for low-dose CT projection data by penalized weighted least-square smoothing in the K-L domain", SPIE Medical Imaging, vol. 4682, pp. 146-152, 2002.

[6] H. Lu, X. Li, L. Li, D. Chen, Y. Xing, M. Wax, and Z. Liang, "Adaptive noise reduction toward low-dose computed tomography, SPIE Medical Imaging, vol. 5030, pp. 759-766, 2003.

[7] G. Wang, S. Zhao, and P-C. Cheng, "Exact and approximate cone-beam X-ray microtomography (Chap. 1)", In Focus on multidimensional microscopy (I). PC Cheng, PP Huang, JL Wu, G Wang, HG Kim, eds, Singapore: World Scientific, pp.233-261, 1999.

[8] G. Wang, C. Crawford, and W. Kalender, "Multi-row detector and cone-beam spiral/helical CT", IEEE Trans Med Imaging, vol. 19, pp. 817-821, 2000.

[9] X. Wang and R. Ning, "A cone-beam reconstruction algorithm for circle-plus-arc data-acquisition geometry cone beam reconstruction", IEEE Trans Med Imaging, vol. 18, pp. 815-824, 1999.

[10] R. Ning, B. Chen, R. Yu, and et al., "Flat panel detector-based cone-beam volume CT angiography imaging: system evaluation", IEEE Trans Med Imaging, vol. 19, pp. 949-963, 2000.

[11] B. Smith, "Cone-beam tomography: recent advances and a tutorial review", Optical Engineering, vol. 29, pp. 524-534, 1990.

[12] J. Liang, H. Lu, J. Wen, T. Li, W. Zhao, J. Hsieh, G. Wang, R. Palermo, "Feasibility studies on low-dose cone-beam 3-D mammography", Proceedings of the VIIth International Conference on Fully 3D Reconstruction in Radiology and Nuclear Medicine, 2003.

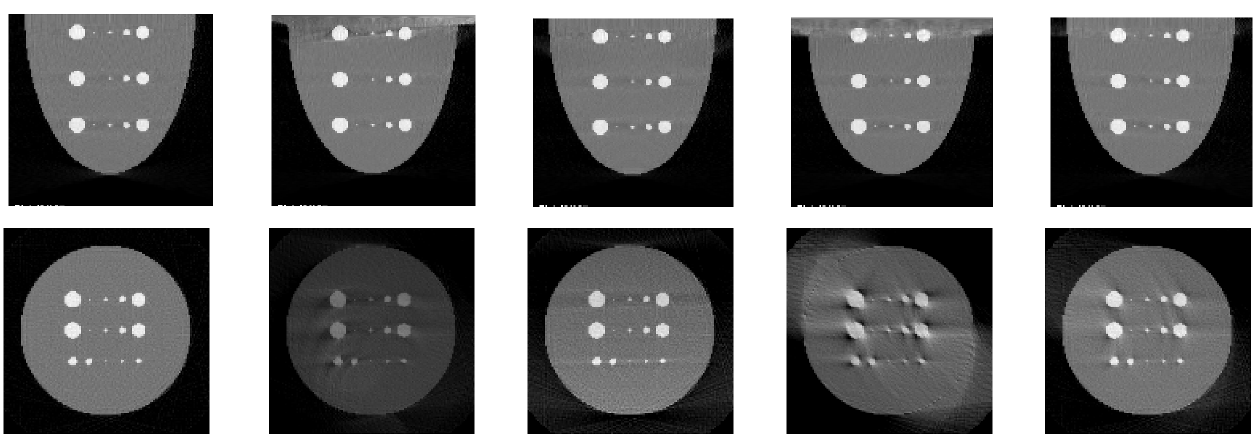

1. circular. 2. spiral. 3. two half-circular. 4. two half-spiral. 5. half-circular+ half-spiral.

Figure 3: Reconstruction results of five orbits, (top is the sagittal view and bottom is the transverse view).

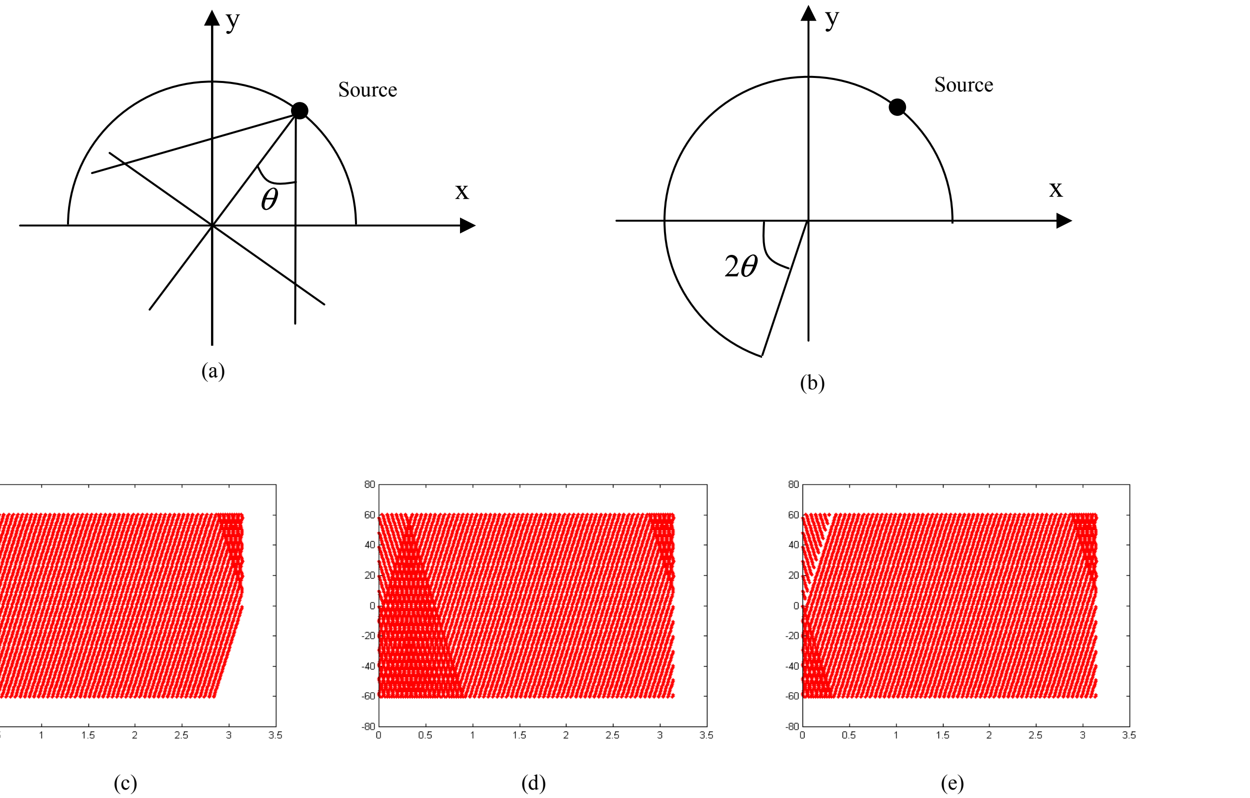

Figure 5: (a) The mid-plane of the cone-beam geometry for 180^o scan. (b) The mid-plane of the cone-beam geometry for 180^o plus added extra scans. (c), (d) and (e) are sampling maps of the mid-plane of the cone-beam geometry for 180^o scan with and without added extra samplings on a circular orbit, where the horizontal axis is the rotating angle ϕ, and the vertical axis is the location x_r. (c) 180^o sampling without added projections. (d) 180^o sampling with added projections (*i.e.*, the fan angles). (e) 180^o sampling with added projections, where the redundant part was eliminated.